



Fourth International Meeting on Wind Turbine Noise

Rome Italy 11-14 April 2011

Time domain modeling of aerodynamic noise from wind turbines

Seunghoon Lee, Soogab Lee

AeroAcoustics and Noise Control Laboratory

School of Mechanical and Aerospace Engineering

Seoul National University, Seoul, Korea

kami00@snu.ac.kr, solee@snu.ac.kr

Abstract

A numerical study was conducted to model the amplitude modulation of the aerodynamic noise from a generic 2.5MW wind turbine. In order to focus on the time-varying characteristics of the wind turbine noise, the aerodynamic noise from the wind turbine is predicted in the time domain. In the present study, the rotor blades are modeled as the combination of a thin rectangular flat plate, and assumed to be moving at zero angle of attack. Since trailing edge noise is known to be the dominant source of the wind turbine noise, the noise prediction only includes this noise source. The acoustic pressure radiated from the blade surface is calculated by using the loading term of Formulation 1A of Farassat. An unsteady surface pressure distribution is analytically derived from the model proposed by Amiet. Validation of the numerical prediction model is also carried out by comparing with an experimental study. By using these numerical methods, the sound pressure level and the modulation depth of wind turbine noise are successfully predicted in this study.

Introduction

Noise from a modern upwind wind turbine is generally lower than that from other environmental noise sources. For a generic 2 MW wind turbine, the A-weighted sound pressure level is about 35 ~ 45 dBA at a distance of 400m from the wind turbine [1]. However, because of its amplitude modulation characteristic, in some circumstance, wind turbine noise is heard even far away from the turbines [2, 3].

Several possible mechanisms for this amplitude modulation were proposed such as noise directivity, excessive wind shear, and blade-tower interaction. However, the cause of the amplitude modulation is still not clearly revealed. Thus, more intensive studies are being required regarding the prediction of the amplitude modulation in wind turbine noise.

Several studies [4, 5] have predicted the amplitude modulation by using the semi-empirical model proposed by Brooks, Pope, and Marcolini [6]. This semi-empirical model provides 1/3 octave band spectra of airfoil self-noise, and it gives good results for predicting the overall sound pressure level and the frequency spectrum of wind

turbine noise [7]. However, it is questionable whether the semi-empirical model is acceptable to calculate the amplitude modulation of wind turbine noise. To predict the amplitude modulation, the temporal variation of wind turbine noise should be predicted properly. However, the semi-empirical model can only predict airfoil self-noise in frequency domain. Moreover, the semi-empirical model uses an inaccurate directivity function for predicting the amplitude modulation. This model employs a cardioid-type directivity function, based on the assumption that the noise is produced from a semi-infinite plate. Although this assumption is reasonable for high frequency component of airfoil self-noise, the cardioid pattern becomes inaccurate as the frequency decreases.

In the present study, in order to model the amplitude modulation of wind turbine noise properly, time-domain modeling of the aerodynamic noise from a wind turbine is carried out. Since turbulent-boundary-layer trailing edge noise is known to be the main source of the wind turbine noise [8], the modeling in this study only includes this noise source. A trailing edge noise model proposed by Amiet [9, 10] is used to model the unsteady surface pressure of a rectangular flat-plate. Far field noise is calculated by using the loading term of Formulation 1A of Farassat [18]. This model is extended to rotor blades based on a strip theory approach. Validation of the numerical prediction model is also carried out with the experimental data of Brooks, Pope, and Marcolini [6].

Trailing edge noise model

In order to predict trailing edge noise in the time domain, unsteady surface pressure should be obtained experimentally or numerically. However, it is difficult to measure or predict the unsteady pressure on wind turbine blade surface. Thus, in the present work, a simplified analytic model proposed by Amiet [9, 10] is used to obtain the unsteady surface pressure. This model is based on thin airfoil theory, and it provides chordwise unsteady pressure distribution for a flat-plate at zero angle of attack. Even though the airfoil is modelled as a flat-plate, this model also gives reasonable results for a slender airfoil [11]. Since most aerodynamic noise is generated at the outboard region, which is rather slender, it seems acceptable to use this model.

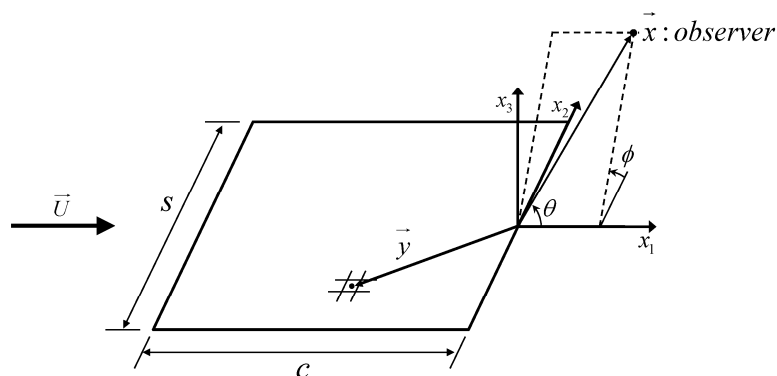


Figure 1 Schematic for a flat-plate model problem

According to this model, the surface pressure jump on the moving surface of a flat-plate, such as Fig. 1, can be expressed as,

$$\Delta p(y_1, y_2, t) = \int_{-\infty}^{\infty} \int_{-\infty}^{\infty} p_0 e^{-i\{k_c(y_1 - U_c t) + k_y y_2\}} \{e^{\varepsilon k_c y_1} - 1 + (1+i)E^*[-y_1(k_c + \mu M + \zeta)]\} dk_c dk_y \quad (1)$$

where, k_c : chordwise convective wave number ($k_c = \omega / U_c$)

k_y : spanwise wave number

U_c : convection velocity

M : Mach number

$E^*[\]$: complex conjugate of Fresnel integral

$e^{\varepsilon k_c y_1}$: exponential convergence factor

$$\zeta = \sqrt{\mu^2 - k_y^2 / \beta^2} \quad \mu = M \omega / \beta^2 U \quad \beta = \sqrt{1 - M^2}$$

Complex conjugate of Fresnel integral, $E^*[\]$ can be numerically calculated as described in Ref. [12]. Equation (1) is the sum of induced surface pressure jump and incident surface pressure jump. The detail descriptions of this equation can be found in Ref. [13].

In order to solve Eq. (1), it is necessary to integrate this equation along two wave numbers. However, since the surface pressure spectrum in the boundary layer is the strongest within the convective ridge centered on $k_c = \omega / U_c$, $k_y = 0$ [14], by assuming that the surface pressure convects as a frozen pattern, it is possible to simplify the equation into

$$\Delta p_c(y_1, y_2, t) \approx \left| \Delta p(y_1, y_2, t) \right|_{k_c = \omega / U_c, k_y = 0} \quad (2)$$

where U_c is a constant convection velocity. The convection velocity is usually $U_c \approx 0.5U \sim 0.7U$, and it is set to $U_c = 0.6U$ in this study. Thus, Eq. (2) becomes

$$\Delta p_c(y_1, t) = \int_{-\infty}^{\infty} p_0 e^{-ik_c(y_1 - U_c t)} \{e^{\varepsilon k_c y_1} - 1 + (1+i)E^*[-y_1\{k_c + \mu(1+M)\}]\} dk_c \quad (3)$$

Next, the numerical integration of Eq. (3) is carried out by the method described in Ref. [11]. Using this method, Eq. (3) is approximated by

$$\Delta p_c(y_1, t) \approx -4\pi \sum_{n=1}^N A_n e^{-i\{k_{c,n}(y_1 - U_c t) + \phi_n\}} \{e^{\varepsilon k_{c,n} y_1} - 1 + (1+i)E^*[-y_1\{k_{c,n} + \mu(1+M)\}]\} \quad (4)$$

where, $A_n = \sqrt{\Phi_{qq}(k_{c,n}, 0) \Delta k_c}$

ϕ_n : independent random variables uniformly distributed on $[0, 2\pi]$

Φ_{qq} : the wall pressure wavenumber-frequency spectrum

$k_{c,N}$: the maximum wavenumber, $\Delta k_c = k_{c,N} / N$ $k_{c,N} = n \Delta k_c$

For a frozen pressure pattern, the wavenumber-frequency spectrum, Φ_{qq} can be written as

$$\Phi_{qq}(k_c, \omega) = \frac{U_c}{\pi} l_y(\omega) S_{pp}(\tilde{\omega}, 0) \quad (5)$$

where $l_y(\omega)$ is the spanwise correlation length, and $S_{pp}(\tilde{\omega}, 0)$ is the wall point pressure frequency spectrum. Several empirical formulas exist for the spanwise correlation length, $l_y(\omega)$, but the formula based on the experimental data of Brooks and Hodgson [15] is applied for this study, as shown in Eq. (6).

$$l_y(\omega) = \frac{U_c}{b\omega} \begin{cases} b = 1.6 & f \leq 750\text{Hz} \\ b = 0.6 & \text{otherwise} \end{cases} \quad (6)$$

According to Ref. [16], for an airfoil the wall point pressure frequency spectrum, $S_{pp}(\tilde{\omega}, 0)$ can be empirically expressed as,

$$S_{qq}(\tilde{\omega}, 0) = \left(\frac{\rho U^2}{2} \right)^2 \frac{\delta^*}{U} S_0(\tilde{\omega}) \quad (7)$$

$$\text{where, } S_0(\tilde{\omega}) = \begin{cases} \frac{1.732 \times 10^{-3} \tilde{\omega}}{(1 - 5.489 \tilde{\omega} + 36.74 \tilde{\omega}^2 + 0.1505 \tilde{\omega}^5)} & \tilde{\omega} < 0.06 \\ \frac{1.4216 \times 10^{-3} \tilde{\omega}}{(0.3261 + 4.1837 \tilde{\omega} + 22.818 \tilde{\omega}^2 + 0.0013 \tilde{\omega}^3 + 0.0028 \tilde{\omega}^5)} & 0.06 < \tilde{\omega} < 20 \end{cases}$$

The boundary layer displacement thickness, δ^* in Eq. (7) can be obtained by an empirical formula for a flat plate [13] or NACA0012 airfoil [6]. However, in the present study, it is numerically obtained by using the XFOIL [17].

Acoustic formulation

Formulation 1A of Farassat [18] is used to obtain the acoustic pressure due to the unsteady surface pressure. Since thickness noise is negligible for the low Mach number [19], only loading noise is calculated in this study. The loading term of Formulation 1A is described as

$$4\pi p'(\vec{x}, t) = \frac{1}{c_0} \int_{f=0} \left[\frac{\dot{l}_i \hat{r}_i}{r(1-M_r)^2} \right]_{ret} ds + \int_{f=0} \left[\frac{l_r - l_i M_i}{r^2(1-M_r)^2} \right]_{ret} ds + \frac{1}{c_0} \int_{f=0} \left[\frac{l_r(r\dot{M}_i \hat{r}_i + c_0 M_r - c_0 M^2)}{r^2(1-M_r)^3} \right]_{ret} ds \quad (8)$$

where, \vec{l} : unsteady surface pressure vector ($\vec{l} = \Re[-\Delta p_c] \hat{n}$)

c_0 : speed of sound

$f = 0$: the surface of the plate

$$\vec{r} = \vec{x} - \vec{y} \quad \hat{r} = \vec{r} / |\vec{x} - \vec{y}| \quad M_r = \vec{M} \cdot \hat{r}$$

$[\]_{ret}$ denotes that the integration is evaluated at the retarded time. Using the equation above, the acoustic pressure at the point \vec{x} at time t can be calculated.

Validation case

Before rotor noise predictions, we first validate the numerical prediction method. The validation is carried out by comparing the result of the experiment of Brooks, Pope, and Marcolini [6]. They performed extensive experiments to measure the airfoil self-noise from NACA0012 airfoil models. The test case of interest here is the tripped boundary layer case of the 2D sharp trailing edge model at zero angle of attack. Since the model has sharp trailing edge and the angle of attack of the test cases is zero, it can be regarded that the dominant source of the airfoil-self noise is trailing edge noise. The span and the chord length of the airfoil model is $s = 0.4572m$ and $c = 0.3048m$, respectively. The inflow velocities of the validation case are 39.6 , 55.5 , and $71.3 m/s$.

For the numerical prediction of the trailing edge noise, the airfoil is modelled as a flat-plate grid which has the same span and chord length with the experiment model. The rectangular surface grid is clustered near the trailing edge, whereas it is uniformly applied in the spanwise direction. The longest chordwise grid is sufficiently small enough to resolve the highest frequency ($max. grid length < \lambda_n/10$). The maximum frequency, f_N of the acoustic prediction is set to $f_N = 10,000Hz$. The frequency range is divided into 1,000 frequencies for the numerical integration. Consequently, the bandwidth (or the lowest frequency) becomes $\Delta f = f_1 = 10Hz$. The calculation is performed during one period of the lowest frequency. Figure 2 shows the predicted acoustic pressure for an inflow velocity of $71.3 m/s$ when the observation position is at $\vec{x} = (0, 0, 1.22)$.

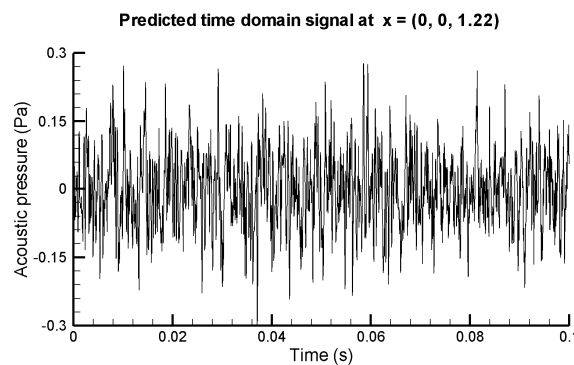


Figure 2 Predicted time domain signal (V=71.3m/s)

Figure 3 demonstrates the comparisons of the 1/3 octave band spectra between the experimental data and the prediction result. Except low frequency region, the sound pressure levels of the numerical prediction agree well with that of the experimental data (within $\pm 3dB$). However, the discrepancy is larger in the mid-to-low frequency

range ($f < 500\text{Hz}$). This is because the basic assumptions of the Amiet's model are less appropriate for the low-frequency range.

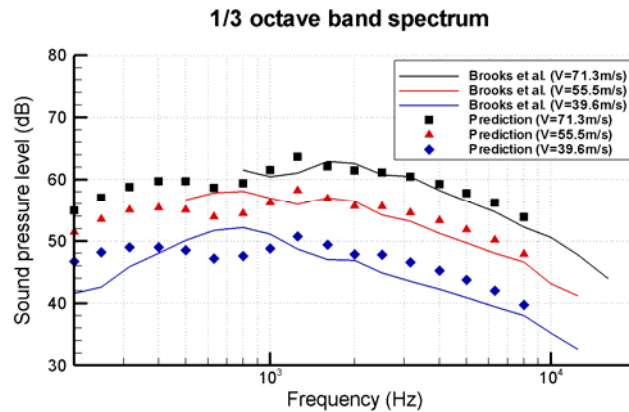


Figure 3 Comparison of 1/3 octave band spectrum

Moreover, the noise directivity of the model airfoil is investigated. First, the acoustic pressure is predicted at each direction in the same way, and then the narrowband spectrum is obtained by applying the fast Fourier transform. The directivity is determined by the RMS value of the frequency spectrum. Figure 4 shows the polar directivity in the mid-span plane for a frequency bands of 100Hz , 500Hz , 1000Hz , and 5000Hz . The thin curve represents the theoretical directivity function for a semi-infinite flat-plate, while the light curves are the noise directivity for the model airfoil. Each curve is normalized by its maximum value. The result is consistent with that of previous studies [20].

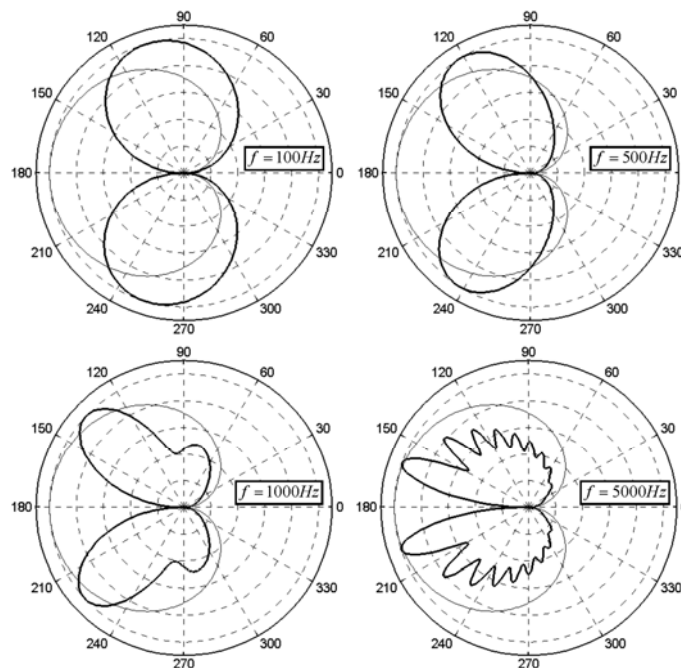


Figure 4 Polar directivity (θ -direction) in the mid-span plane

Rotor noise prediction

The wind turbine model used here is a generic 2.5MW 3-blade wind turbine, which has typical multi-MW wind turbine characteristics. This turbine is pitch regulated, variable speed type with a rotor diameter of 93 m and a hub height of 82 m . It reaches a maximum rotational speed of 15.4 RPM at a wind speed of 9 m/s , and its rated power is 2.5MW at a wind speed of 11.5 m/s .

In order to apply the trailing edge noise model for a rectilinear motion to the rotating blades, a strip theory approach is used. First, each blade is divided into 20 segments, and each segment is modelled as a rectangular flat-plate. Next, the trailing edge noise model is applied to each segment. Each segment assumed to move rectilinearly at zero angle of attack; the inflow velocity to each segment is assumed to be the rotational velocity based on the center of the segment.

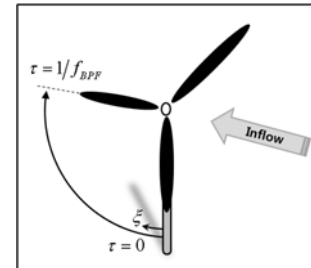


Figure 5 Wind turbine model

Figure 5 demonstrates the direction of rotor rotation and the rotor position at $\tau = 0$. The calculation is performed for a duration of 1/3 revolution of the turbine ($T = 1/f_{BPF}$). The maximum frequency and the frequency bandwidth are set to $f_N = 2,500Hz$ and $\Delta f = 10Hz$, respectively. High frequencies ($f > 2500Hz$) are not predicted in this study, because not only they are easily attenuated by air absorption, but the computation cost will increase rapidly as the maximum frequency, f_N increases.

Result and Discussion

Figure 6 presents the predicted acoustic pressure at the reference positions according to IEC 61400-11. The overall sound pressure levels and the A-weighted sound pressure levels are also shown in the figure.

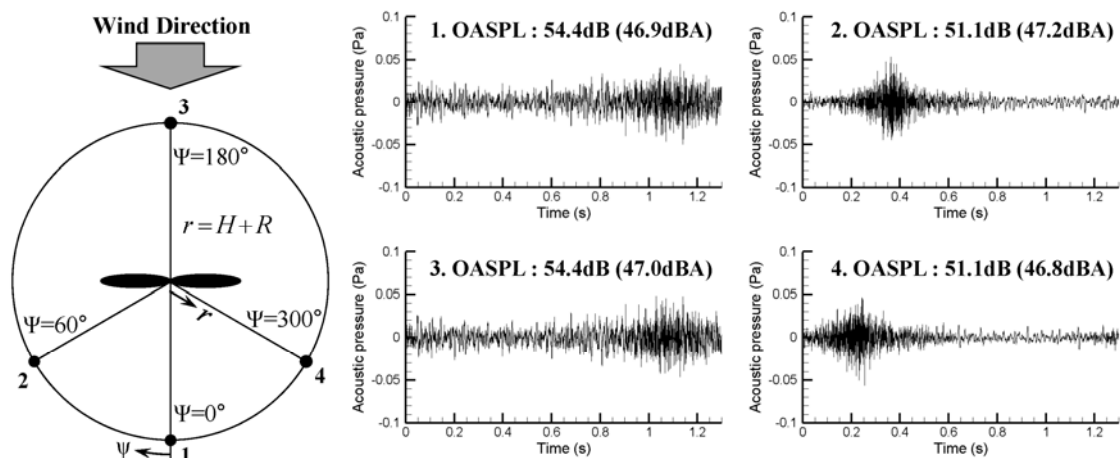


Figure 6 IEC 61400-11 Reference position: Acoustic pressure

Since the effect of angle of attack is not included in this prediction procedure, the result may underestimate the noise level from wind turbines. Instead, this result clearly shows that the amplitude modulation of wind turbine noise exists for all of the observer positions. In order to assess the strength of this amplitude modulation, first of all, the predicted acoustic pressure is divided into two signals by the shifting procedure described in Fig. 7.

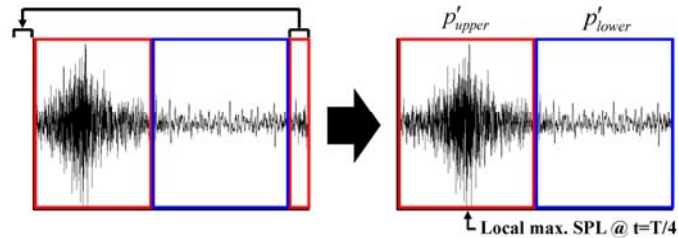


Figure 7 Division into upper and lower acoustic pressure

Next, 1/3 octave band spectra is obtained for upper, lower, and total acoustic pressure at position 1 and 2, as shown in Fig. 8. The blue bars represent the average 1/3 octave band spectra, whereas the black and red bars mean the 1/3 octave band spectra of the lower and upper acoustic pressure, respectively. The average spectrum of the acoustic pressure at position 1 is similar to that of the acoustic pressure at position 2, except in the range of $100 \sim 200\text{Hz}$ and $800 \sim 1250\text{Hz}$; the low frequency spectrum at position 1 is slightly higher than the spectrum at position 2, and the mid-frequency spectrum at position 2 is a little higher than the spectrum at position 1. However, the modulation depth, which is defined as the difference between the upper and lower spectrum, is different between the observer positions. The modulation depth at position 2 is much higher than the modulation depth at position 1. These differences increase as the center frequency increases. This is due to the difference of the noise directivity between low and high frequencies, as presented in Fig. 4.

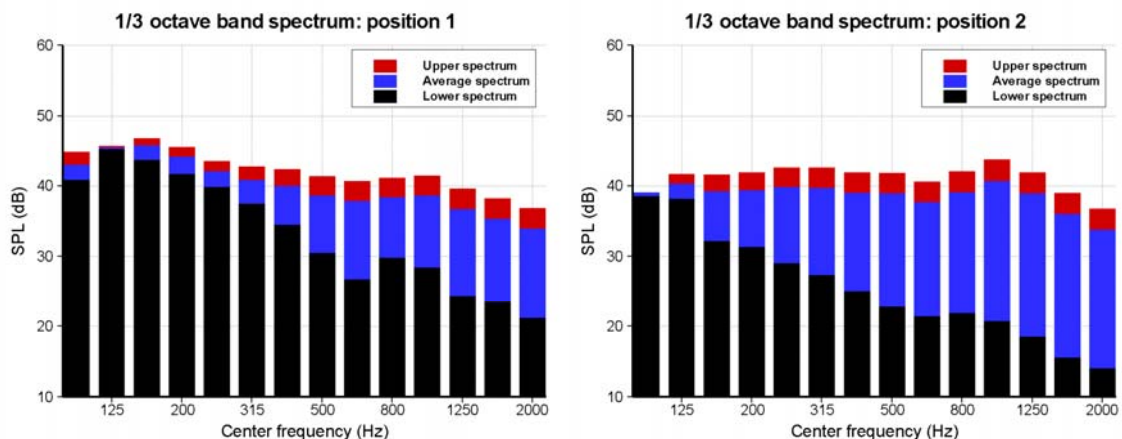


Figure 8 1/3 octave band spectra of total, upper, and lower acoustic pressure

Moreover, in order to evaluate the sound pressure level and the modulation depth at far distances from the wind turbine, the acoustic pressure is calculated for the downwind positions ($-90^\circ < \psi < 90^\circ$) at a distance of $250m$, $500m$, $750m$, and $1000m$ from the wind turbine. These acoustic signals are then converted to 1/3 octave band spectra ($f_c = 100 \sim 2000Hz$) as the procedure in Fig. 7 and 8. Next, to include the effect of atmospheric attenuation, the sound pressure levels at each frequency band are subtracted from the attenuated sound levels, which are determined as the multiplication of attenuation coefficients [21] and the distance between the rotor hub and the observer point. The air temperature, the relative humidity, and the air pressure are assumed as $15^\circ C$, 60% , and 1 atm , respectively. The overall sound pressure levels and the overall modulation depths for the 1/3 octave band spectra are plotted in Fig. 9.

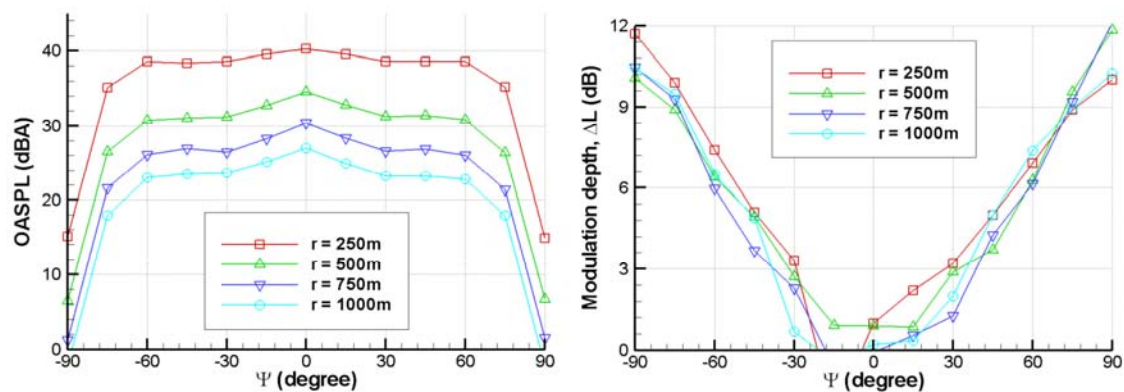


Figure 9 Overall sound pressure level and modulation depth

It is found that the sound pressure level is maximum at downwind direction ($\psi = 0^\circ$), but it is minimum at crosswind direction ($\psi = \pm 90^\circ$). On the other hand, the modulation depth is largest at crosswind direction, but the amplitude modulation does not exist at downwind direction. Furthermore, it is worthy of notice that at far distances (e.g. $r > 250m$) the modulation depth is consistent with increasing the distances, while the overall sound pressure level decreases by about 6dB per distance doubling. This is because the variation range of the directivity angles (θ , ϕ in Fig. 1) is invariant with the distances.

Perception of AM at far distances

Figure 10 presents the directivity angles with respect to rotor azimuth, ξ , when an observer is assumed to be located at far distance from the turbine (e.g. $r = 1,000m$). The rotor azimuth angle is defined as described in Fig. 5. The directivity angles in Fig. 10 are calculated at the outward segment of the blade.

Figure 10 clearly shows why the amplitude modulated sound is produced due to the variation of the directivity angles. Even though an observer is located far from the turbine, θ and ϕ vary considerably as the rotor rotates. This leads to the variation of the sound pressure level of trailing edge noise. Moreover, this variation increases as

the observer is closer to the rotation plane. When the observer is located at the downwind position ($\Psi = 0^\circ$), the differences between the maximum angles and the minimum angles are less than 10° . However, if the observer is located near the rotation plane (e.g. $\Psi = 75^\circ$), these differences can reach up to 150° . This is why the modulation depth is largest at crosswind direction, as shown in Fig. 9.

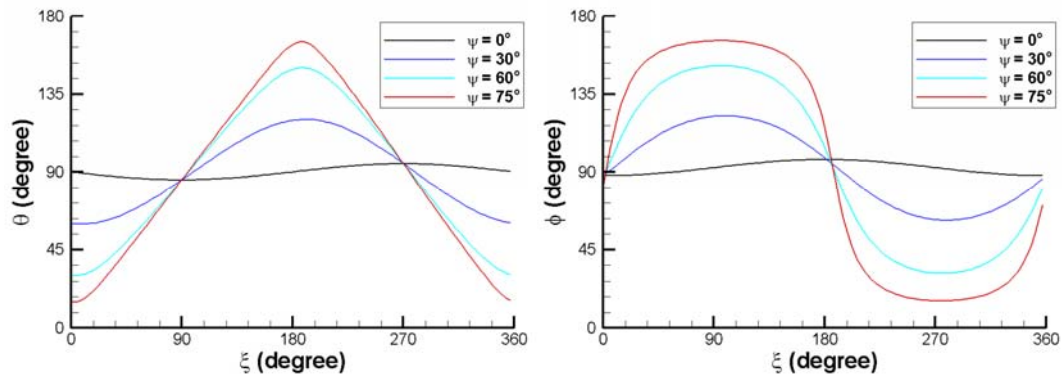


Figure 10 Variation of directivity angles with respect to rotor azimuth

Nevertheless, although the modulation depth is large near the rotation plane, there is little possibility of perceiving the sound in this direction, because the sound pressure level is too low; the overall sound pressure level is less than 10dBA in crosswind directions. On the other hand, in downwind direction, even though the sound pressure level is relatively high, the amplitude modulation does not exist. Thus, this sound will be easily masked by background noise. However, the amplitude modulation may be perceived in the range of about $\Psi \approx \pm 30 \sim \pm 60^\circ$. In this direction, not only the amplitude modulation exists, but also the sound level is not very low even far away from the turbine. Therefore, there is a possibility of perceiving the amplitude modulation in this direction, if the background level is quiet low (e.g. less than 30dBA).

Conclusion

This study predicted the aerodynamic noise from a generic 2.5MW wind turbine in time domain to model the amplitude modulation of wind turbine noise. A trailing edge noise model for a rectilinear motion is used to obtain the unsteady surface pressure on a flat-plate surface. This noise model for a flat-plate is extended to the rotor blade based on a strip theory approach.

By applying this numerical method to the model rotor, the acoustic pressure radiated from the wind turbine blade is successfully predicted in this study. Moreover, using predicted acoustic pressure, 1/3 octave band spectra and its modulation depth can be obtained at far distance from the turbine. The result showed that the amplitude modulation is largest at crosswind direction, but it does not exist at upwind and downwind direction. It is also found that at far distances the modulation depth does not decrease with increasing the distance.

Acknowledgements

This work was supported by the Human Resources Development of the Korea Institute of Energy Technology Evaluation and Planning (KETEP) grant funded by the Korea government Ministry of Knowledge Economy (No. 20094020100060).

This work was also supported by the New and Renewable Energy of the Korea Institute of Energy Technology Evaluation and Planning (KETEP) grant funded by the Korea government Ministry of Knowledge Economy (No.20104010100490).

References

- [1] S. Wagner, R. Bareiß, and G. Guidati, *Wind Turbine Noise*, Springer (1996)
- [2] G.P. van den Berg, "Effect of the wind profile at night on wind turbine sound", *Journal of Sound and Vibration*, vol. 277, p. 955-970 (2004)
- [3] D. Bowdler, "Amplitude modulation of wind turbine noise", *Acoustics Bulletin of the Institute of Acoustics*, vol. 33 (4), July/August (2008)
- [4] S. Oerlemans and J. G. Schepers, "Prediction of wind turbine noise and validation against experiment", *International Journal of Aeroacoustics*, vol. 8 (6), p. 555-584 (2009)
- [5] S. Lee, H. Kim, K. Kim, S. Lee, "Perception of amplitude-modulated noise from wind turbines", *Proc. ICSV 17* (2010).
- [6] T. F. Brooks, D. S. Pope, and M. A. Marcolini, "Airfoil self-noise and prediction", NASA reference publication 1218, July 1989
- [7] W. J. Zhu, N. Heilskov, W. Z. Shen, and J. N. Sørensen, "Modeling of aerodynamically generated noise from wind turbines", *Journal of Solar Energy Engineering*, vol. 127, p. 517-528 (2005)
- [8] S. Oerlemans, P. Sijtsma and B. Méndez López, "Location and quantification of noise sources on a wind turbine", *Journal of Sound and Vibration*, vo. 299 p. 869-883 (2007)
- [9] R. K. Amiet, "Noise due to a turbulent flow past a trailing edge", *Journal of Sound and Vibration*, vol. 47 (3), p. 387-393 (1976)
- [10] R. K. Amiet, "Effect of the incident surface pressure field on noise due to a turbulent flow past a trailing edge", *Journal of Sound and Vibration*, vol. 57 (2), p. 305-306 (1978)
- [11] J. Casper and F. Farassat, "Broadband trailing edge noise predictions in the time domain", *Journal of Sound and Vibration*, vol. 271, p. 159-176 (2004)
- [12] J. Boersma, "Computation of Fresnel integrals", *Mathematics of Computation*, Vol. 14, (72), p. 380 (1960)
- [13] R. H. Schlinker, and R. K. Amiet, "Helicopter rotor trailing edge noise", NASA Contractor Report No. 3470 (1981)
- [14] M. S. Howe, *Acoustics of fluid-structure interactions*, Cambridge (2008)

- [15] T. F. Brooks and T. H. Hodgson, "Trailing edge noise prediction from measured surface pressures", *Journal of Sound and Vibration*, vol. 78 (1), p. 69-117 (1981)
- [16] S. T. Chou and A. R. George, "Effect of angle of attack on rotor trailing-edge noise", *AIAA Journal*, vol. 22 (12), p. 1821-1823 (1984)
- [17] M. Drela, XFOIL: An analysis and design system for low Reynolds number airfoils, *Conference on Low Reynolds Number Aerodynamics*, University of Notre Dame, June (1989)
- [18] Farassat, F. and Succi, G. P., "The prediction of helicopter rotor discrete frequency noise", *Vertica*, vol. 7 (4), p. 309-320 (1983)
- [19] Q. Zhou and P. Joseph, "A frequency domain numerical method for airfoil broadband self-noise prediction", *Journal of Sound and Vibration*, vol. 299, p. 504-519 (2007)
- [20] M. S. Howe, "Edge-source acoustic Green's function for an airfoil of arbitrary chord, with application to trailing-edge noise", *The Quarterly Journal of Mechanics and Applied Mathematics*, vol. 54 (1), p. 139-155 (2001)
- [21] ISO 9613-1, *Acoustics – Attenuation of sound during propagation outdoor—Part 1: Calculation of the absorption of sound by the atmosphere*, International Organization for Standardization (1993)